GRAPHENE OXIDE BASED TRANSPARENT RESINS FOR ACCURATE 3D PRINTING OF CONDUCTIVE MATERIALS

David Tilve-Martínez, Wilfred Neri, Dylan Horaud, Nicolas Vukadinovic, Benoit Berton, Jinkai Yuan, Philippe Poulin**

D. Tilve-Martínez, W. Neri, D. Horaud, J. Yuan, P. Poulin
Univ. Bordeaux
CNRS, CRPP, UMR5031
115 Avenue Dr. Albert Schweitzer
Pessac 33600, France
david.tilve@crpp.cnrs.fr
philippe.poulin@crpp.cnrs.fr

N. Vukadinovic, B. Berton
Dassault Aviation
78 quai Marcel Dassault
Saint-Cloud 98552, France

Keywords: 3D printing, nanocomposites, graphene oxide, conductivity.

ABSTRACT

Digital Light Processing (DLP) allows the fast realization of 3D objects with high spatial resolution. However, DLP is limited to highly transparent resins, and therefore not well suited for printing electrically conductive materials. Manufacturing conductive materials would significantly broaden the spectrum of applications of the DLP technology. But conductive metal or carbon based fillers absorb and scatter light; inhibiting thereby photopolymerization, and lowering 3D printing resolution. In this work, UV transparent liquid crystal graphene oxide (GO) is used as precursor for generating *in-situ* conductive particles. The GO materials are added to a photopolymerizable resin via an original solvent exchange process. By contrast to earlier contributions, the absence of drying during the all process allows the GO material to be transferred as monolayers to limit UV scattering. The absence of UV scattering and absorption allows for fast and high-resolution 3D printing. The chosen resin sustain high temperature to enable an *in-situ* efficient thermal reduction of GO into reduced graphene oxide rGO which is electrically conductive. The rGO particles form percolated networks with conductivities up to $1.2 \cdot 10^{-2}$ S·m^{-1}. The present method appears therefore as a way to reconcile the DLP technology with the manufacturing of 3D electrically conductive objects.

1. Introduction

Digital Light Processing (DLP)[1] is an additive manufacturing technology generally limited to transparent photocurable resins. Transparency is required to ensure fast and spatially accurate photopolymerization upon UV irradiation. Unfortunately, the requirement of transparency makes the processing of electrically conductive resins difficult. Manufacturing conductive materials would broaden the spectrum of applications of the DLP[2–4] by allowing the fabrication of 3D objects with sensing, actuating, or communicating functionalities.

The addition of electrically conductive filler in a polymer matrix is a common strategy to make an initially insulating polymer conductive[5–8]. Classical conductive fillers include metal or carbon micro- or nano-particles. The particles must be sufficiently concentrated to form a connected and conductive network. Their volume fraction must be above the so-called percolation threshold to achieve a sufficiently high conductivity[9]. A high percolation threshold is associated with a substantial loss of transparency because conductive particles absorb and scatter UV light.

In this context, anisotropic particles such as rod-like or plate-like particles have been used in the last years to make 3D printable resins. Anisotropic particles are used because they display a percolation threshold lower than spherical or quasi-spherical particles[9–11]. Multi-Walled Carbon Nanotubes (MWCNTs) for example have been used in recent work[12–15]. However, the formulations contain aggregates that can settle in the long term, and make 3D printing more difficult. Besides, above the percolation threshold, the quality of 3D printing decreases because of scattering and defects. Graphene Nano-Platelets (GNP) [16],[17] have also been tested but with lower conductivity or greater percolation threshold compared to nanotubes. Dried reduced graphene oxide (rGO) has also been used as conductive fillers for DLP applications[18]. However, GO layers tend to stack and aggregate irreversibly upon drying[19–23]. GO powders in water have also been added to low molecular weight water-soluble poly (ethylene glycol)diacrylate (PEGDA) resins for 3D printing applications[24]. This approach is interesting because GO absorbs much less UV than rGO[5,6]. However, the method is limited to water-miscible PEGDA resins which unfortunately do not sustain high-temperature treatments for efficient reduction of GO. The obtained materials remain therefore poorly conductive with conductivities on the order of 10^{-7} S m^{-1}.

In the present work, we use GO monolayers as precursor particles. In contrast to previous studies, GO is used during 3D printing in its neat oxidized state and never dried during all processes. Neat and undried GO monolayers enjoy several advantages. They display a low

percolation threshold because of their plate-like shape and giant aspect ratio[25]. Their UV absorption is lower than that of other conductive particles generally used for making conductive composites, including rGO[5,6]. Neat GO is insulating but can be easily made conductive by an *in-situ* thermal or chemical reduction after 3D printing[19] if dispersed in a robust resin that can sustain the reduction treatments. In this work, we use acrylic resins that can be heated up to 300°C, ensuring an efficient reduction of GO.

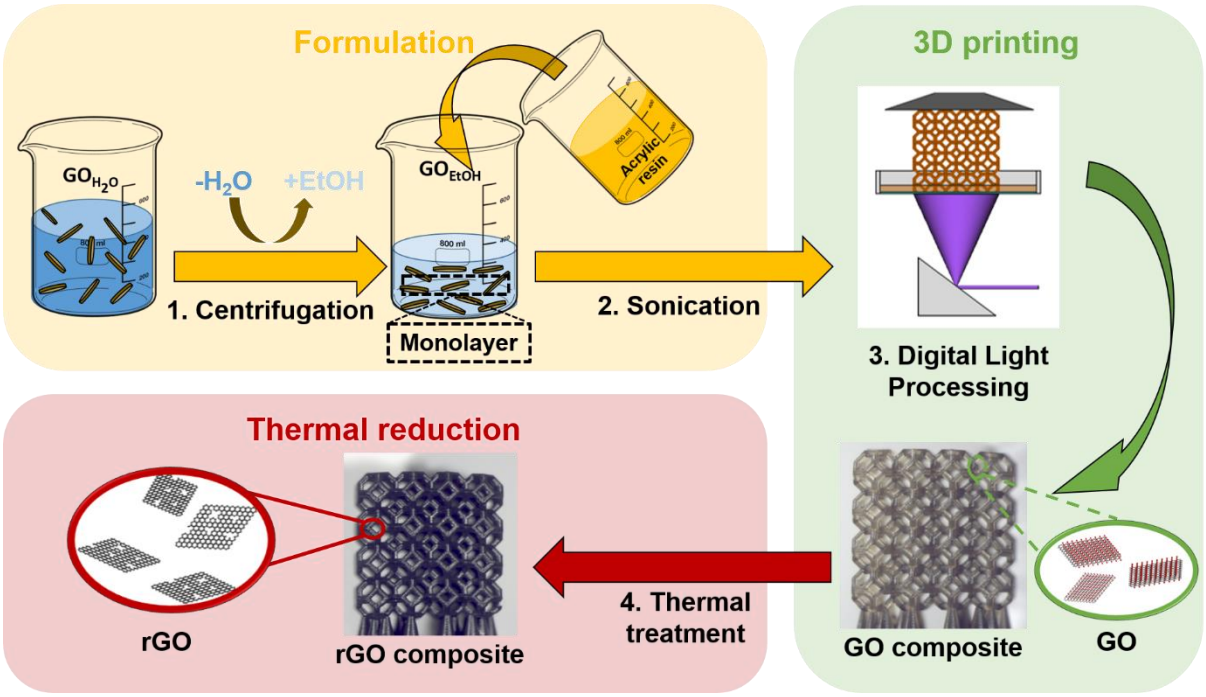

Figure 1. Scheme of the GO-based composites manufacture by Digital Light Processing. A monolayer GO dispersion is added to the resin and then, by UV 2D projections, the formulation is 3D printed. A final thermal post-treatment is applied in order to reduce GO and obtained a conductive composite.

We take advantage of the solubility of GO monolayers in ethanol, and of the miscibility of ethanol and acrylic resins to transfer GO atomic monolayers from water to the resin (Figure 1). For this, we initially prepared a concentrated GO liquid crystal ethanol solution by a phase transfer method. This GO liquid crystal solution is mixed with a resin that can withstand high temperatures. The formulation is then 3D printed by DLP. It is thermally treated to reduce the GO, and finally obtain a conductive 3D-printed nanocomposite. The use of undried GO materials allows accurate and fast printing. The low percolation threshold (0.05% wt) and the efficient reduction of GO lead to materials with enhanced electrical conductivity, with conductivities on the order of 10^{-2} S m^{-1}, largely above those of related materials[18,24]. We also

qualitatively show that the present method allows much better resolution when compared to 3D printing using rGO or nanotube materials.

2. Results and Discussion

2.1. Formulation and 3D printing of GO composites

Manufacturing of a conductive GO-based composite by DLP requires the formulation of a stable and homogeneous dispersion in the acrylic matrix in order to have a material sufficiently transparent to UV light at 405 nm. As shown in Figure 2, GO is a weak UV-visible absorber. It is therefore well appropriate for DLP. In contrast, as most conductive fillers, rGO obtained after reduction is a much stronger UV absorber, less appropriate for DLP in spite of being electrically conductive

.

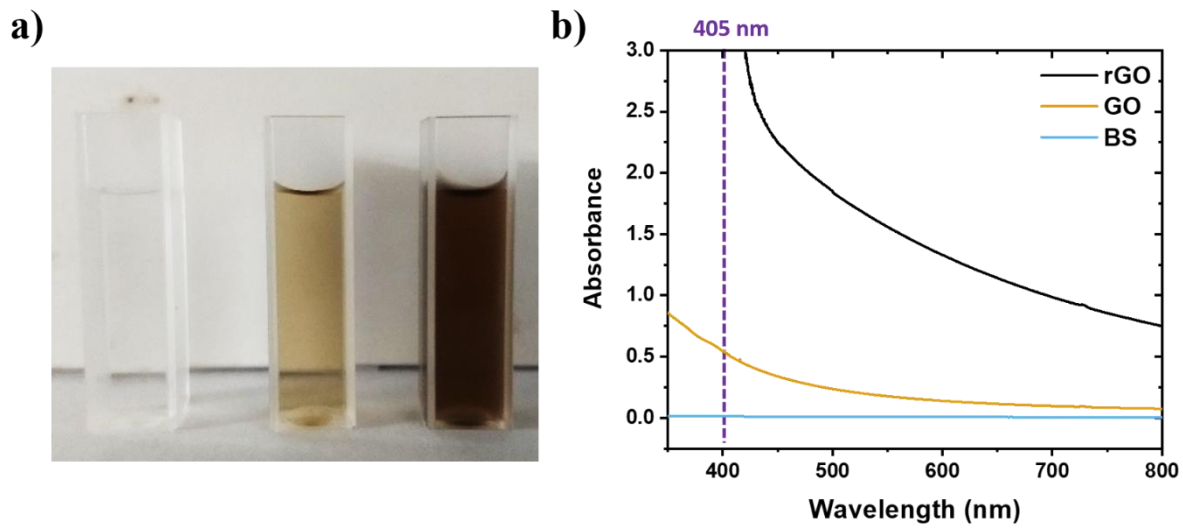

Figure 2. **a)** Poly(methyl methacrylate) (PMMA) cuvettes containing (from left to right) distilled water, 0.005% wt GO dispersed in water, 0.005% wt rGO stabilized with 0.35% wt bile salt (BS), **b)** Absorbance spectra of the (black) rGO dispersions, (brown) GO, and (blue) BS solution.

Besides, directly adding rGO to the resin and using a tip sonication results in a poor dispersion with irreversible aggregates formed during reduction. As can be seen in Figure 3 (a), the aggregate size spans from a few microns to 50 microns. Instead, a homogeneous liquid crystal solution of GO atomic monolayers forms in ethanol (Figure 3b). This concentrated solution is added to the acrylic resin by taking advantage of the high solubility of ethanol in the resin. This results in a homogeneous and stable dispersion of the GO monolayers inside the matrix (Figure 3 c, d). The absence of aggregation is revealed in the optical micrographs by the absence of large black particles.

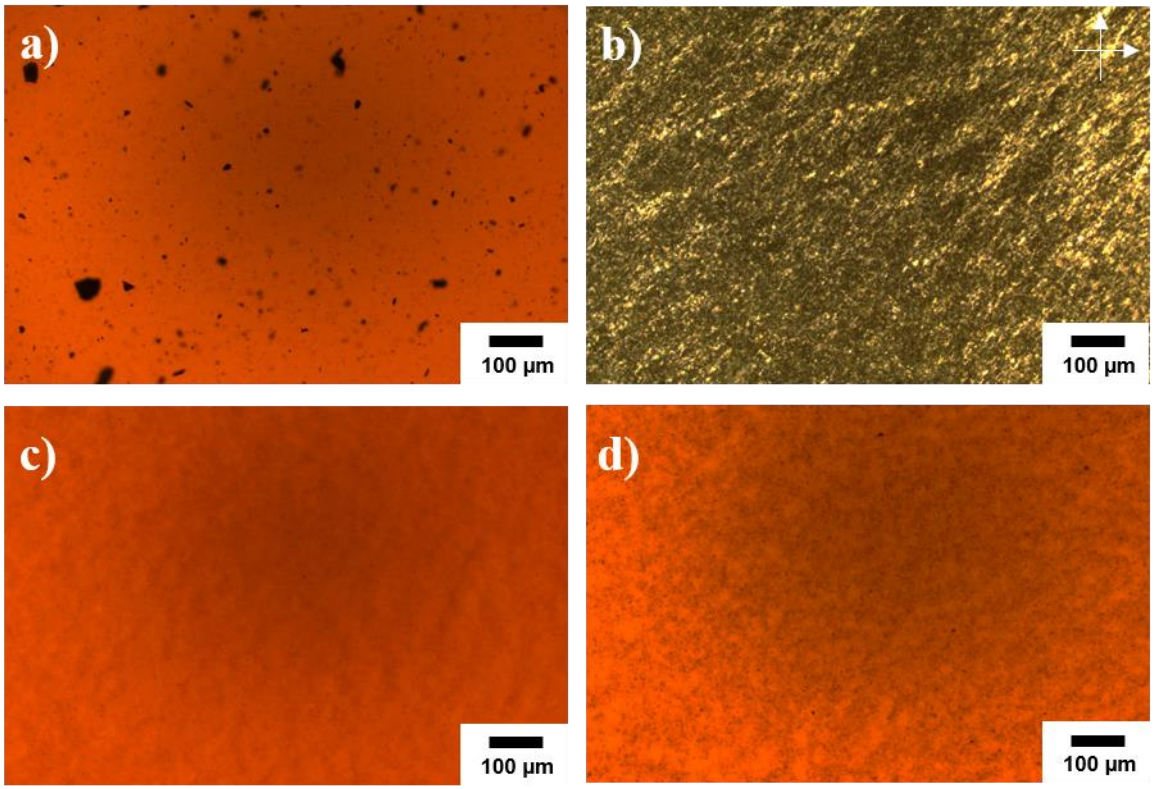

Figure 3. Optical micrographs of the dispersions: **a)** 0.3 wt % rGO in the acrylic resin, **b)** GO ethanol-rich solution at 2.4 wt % under crossed polarizers. The axes of the polarizers are shown by white arrows. Birefringence reveals the liquid crystallinity of the solution **c)** 0.25 wt % and **d)** 0.45 wt % GO in the acrylic resin.

Dispersion rheology is particularly useful to optimize 3D printing. A viscosity of 3 to 5 Pa·s at a shear rate of 10 s^{-1} is considered as an upper limit for the DLP of ceramics[26–28]. This condition is necessary to facilitate the coating and self-leveling of the resin. It avoids also the formation of bubbles that could lead to printing failure. The neat resin used in this work has a Newtonian behavior. But a strong shear-thinning behavior is observed as soon as GO is added to the resin (Figure 4). The viscosity increases with the fraction of GO. The viscosity at 10 s^{-1} is 3.94 Pa·s for a filler concentration of 0.35% wt . This viscosity is lower than 5 Pa·s estimated as an upper limit for ceramic materials[28]. The viscosity of the 0.45% wt GO formulation is 9.38 Pa·s which slightly overcomes this limit. But this viscosity level remains on the same order of magnitude, meaning that our present materials still remain 3D printable.

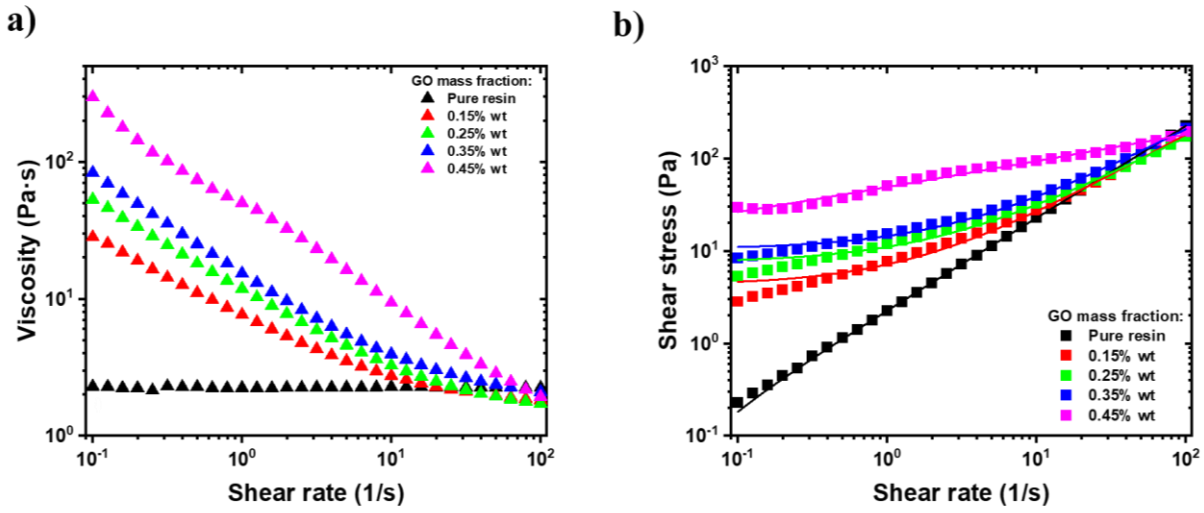

Figure 4. a) Viscosity and **b)** shear stress as a function of shear rate for the acrylate resins containing different weight fractions of GO.

The efficiency of photopolymerization can be evaluated by the so-called Jacobs model[42]. In this model, C_d, the depth of polymerization, is plotted as a function of E_0 (mJ cm^{-2}) the irradiation energy, and the data are fitted according to Equation (1).

$$C_d = D_p \, ln\left({E_0}/{E_c}\right) \quad (1)$$

E_c (mJ cm^{-2}) is a characteristic energy associated with the crosslinking of the polymer. D_p (µm) is the so-called penetration depth. This semi-logarithmic working curve results from the Beer-Lambert relation. It allows the printing parameters to be optimized, and the printing limitations of the DLP technique to be determined.

Commercial DLP resins are highly transparent at 405 nm to allow for efficient photo-induced cross-linking reactions. The addition of fillers can affect the process because of light scattering and absorption[26,27]. GO sheets can also induce free radical trapping of acrylic chains by reacting with the sp^2 carbons of GO[29,30]. This effect also limits the cross-linking mechanisms. The influence of the above phenomena on DLP can be quantified by the determination of the Jacobs working curves. Figure 5 shows how the presence of fillers in the matrix limits the penetration depth of light (D_p). D_p decreases clearly with increasing the weight fraction of GO in the resin. Nevertheless, printing remains easily doable thanks to the weak UV absorption and limited scattering of neat GO monolayers. Determination of the Jacobs curves provides key information to set optimal printing parameters, as indicated in the next section.

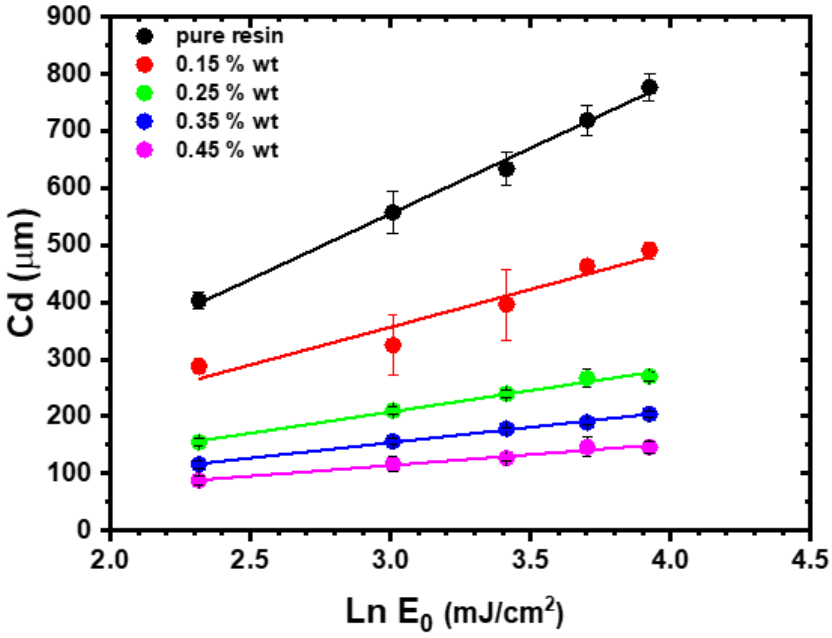

Figure 5. Jacobs working curves for composites with different GO weight fractions at 405 nm (1.27 mW cm^{-2}). C_d is the depth of polymerization. E_0 is the irradiation energy.

2.2. DLP of GO and rGO composites

Knowing all these details, we are able to optimize the time of exposure depending on the GO loading in our formulation. Figure 6 shows a CAD model of a complex cellular structure which has been 3D printed using 0.15% wt of GO and 0.15% wt MWCNTs respectively. According to the Jacobs equation (1), 1.5 mJ cm^{-2} (equivalent to 4.5 s) must be irradiated to 3D print a 50 μm layer for a 0.15% wt MWCNTs formulation (Figure 2S). In our case, if we irradiate 1.5 mJ cm^{-2} for a 0.15% wt GO formulation the layer thickness 3D printed is 150 μm. As can be seen, the structure 3D printed with GO is flawless and has a remarkable resolution because of its transparency. By contrast, the structure printed with carbon nanotubes at the same concentration display several defects, in the finest areas that require greater precision[31].

The optical micrograph of the carbon nanotube dispersions (Figure 3S)) shows aggregates bigger than 50 μm. Even setting an exposure time of 2.3 mJ cm^{-2} (equivalent to 10 s) still leads to defects and failures in the process. Those come from the strong UV absorption of nanotubes and from their difficult dispersion with aggregates that can be as large as the printing layers. UV transparent GO formulations at the monoatomic level can be printed faster with better resolution.

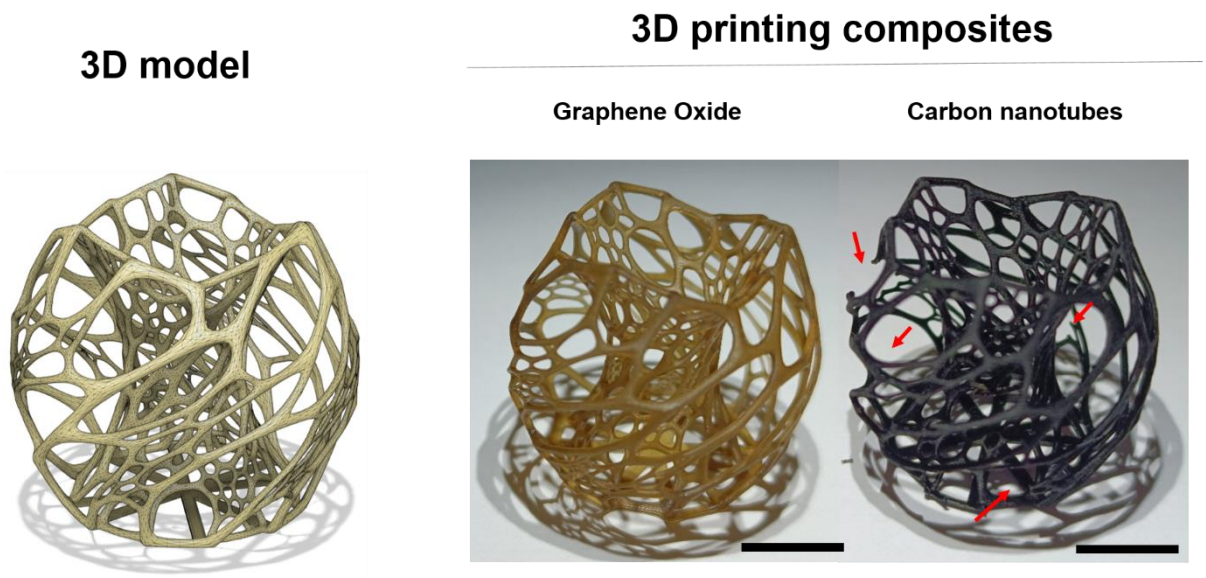

Figure 6. Digital model of a complex structure and photographs of a 3D printed of 0.15 wt % GO composite and 0.15 wt % MWCNTs composite. Red arrows show the failures during the 3D printing process. Scale bars: 1 cm

For other characterizations, 2x2x2 mm^3 cubes were printed. Figure 7 shows how the color of the resin changes with the addition and reduction of GO particles. Thermogravimetric analysis (Figure S1) under a flow of oxygen shows that the resin sustains temperatures up to 300 ºC with a weight loss of only 4%. This high resistance to temperature allows the GO to be effectively reduced by thermal annealing. After heat treatment at 200 ºC, the object turns actually to a dark black color. The maximum GO weight fraction of printed composites was 0.55%. At this high weight fraction, and already above 0.45% wt, the printing quality decreases. At 0.45% wt of GO, our formulations meet the rheological limits of 3D printing found empirically for ceramic composites. Moreover, the Jacobs working curves show a clear decrease in the 3D printing depth, associated to a more difficult printing.

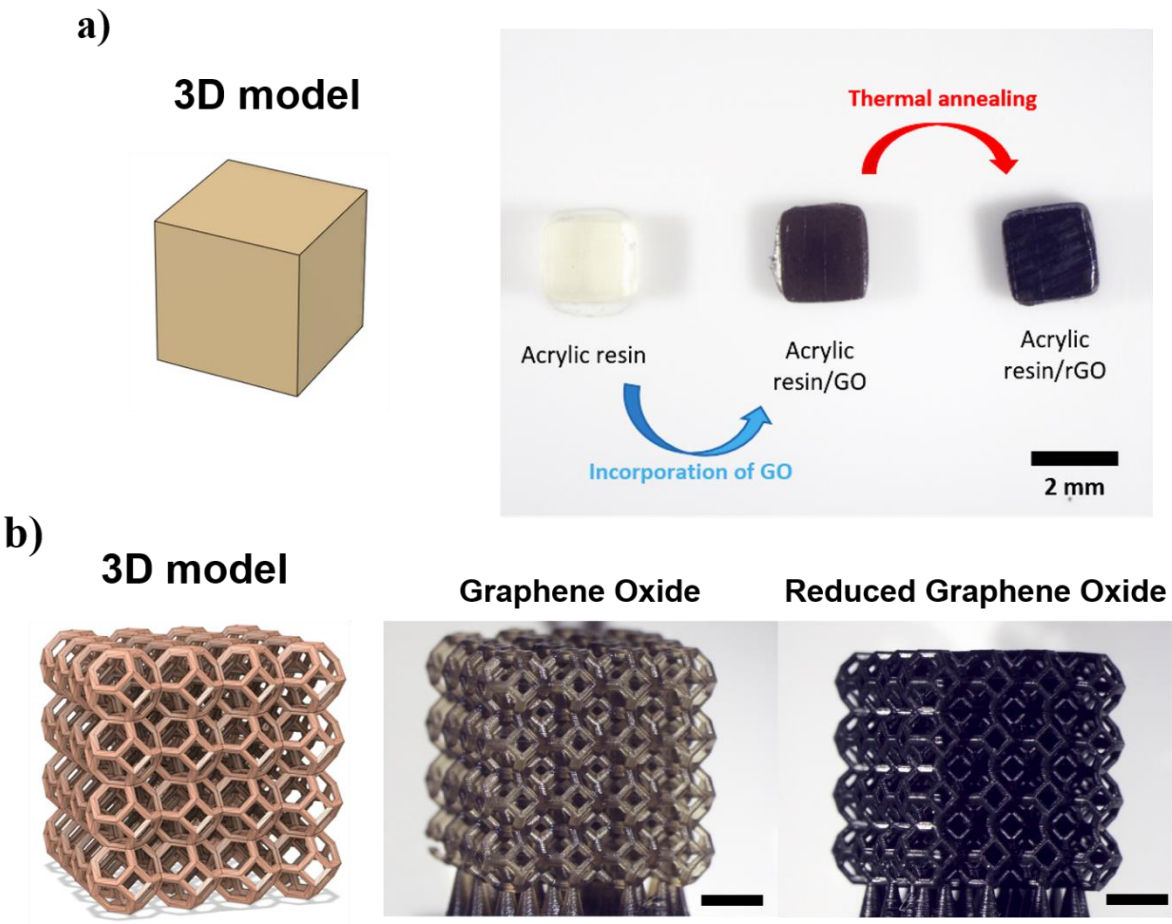

Figure 7. **a)** 3D printed cube structures from left to right: pristine resin (transparent-yellow color), GO composite (dark brown color) and rGO composite (black color), **b)** 3D printed 4x4x4 tetrakaidecahedron cells of 0.35% wt GO composite before and after thermal reduction. Scale bars: 3 mm

2.3. Mechanical properties

Samples of the type ASTM D638 Type IV have been manufactured by 3D printing for the characterization of mechanical properties. The properties have been studied as a function of three parameters: the ethanol content in the resin, the GO weight fraction, and the thermal treatment.

The as-printed composite materials display a lower stiffness and greater strain at break than as-printed neat resins. This behavior is likely due to the presence of ethanol in the composite resin during 3D printing. Ethanol can indeed limit the degree of cross-linking. The Young's modulus of the neat cross-linked resin is 10.8 ± 0.9 GPa. This modulus is reduced by half with the addition of only 5% wt ethanol in the same conditions of UV irradiation.

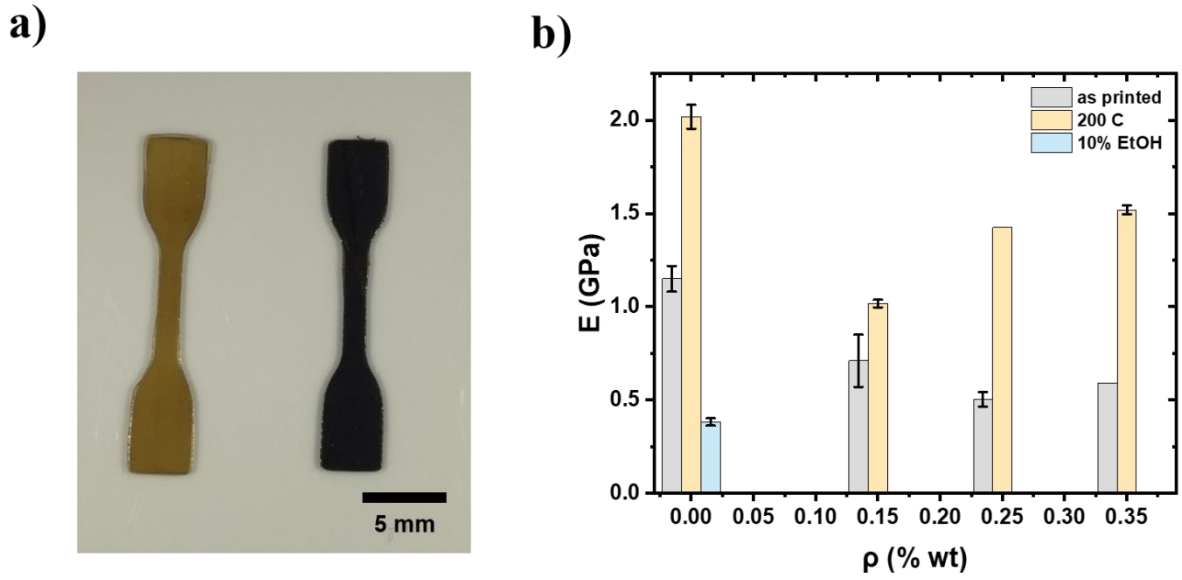

Figure 8. **a)** Photograph of the tensile test samples before (left) and after (right) thermal reduction and **b)** Young's moduli of the composites after and before thermal annealing as a function of GO fractions.

Young's modulus increases after the reduction treatment of GO. This increase is more likely due to an improved curing of the resin upon thermal treatment, rather than to an increase in the stiffness and reinforcement efficiency of the rGO particles. Because even without GO additives, the neat resin also presents a significant improvement in Young's modulus after the thermal treatments.

2.4. Electrical properties

Printed composites are found to be conductive after the in-situ reduction treatment of GO. The conductivity of the samples as a function of the weight fraction of GO is shown in Figure 9. The data are fitted using the following percolation scaling equation:

$$\sigma = \sigma_0 \, (\rho - \rho_c)^t \qquad (2)$$

where σ_0 is a scaling factor (S/m), ρ is the weight fraction of filler (wt %), ρ_c is the percolation threshold (wt %) and t is a critical exponent.

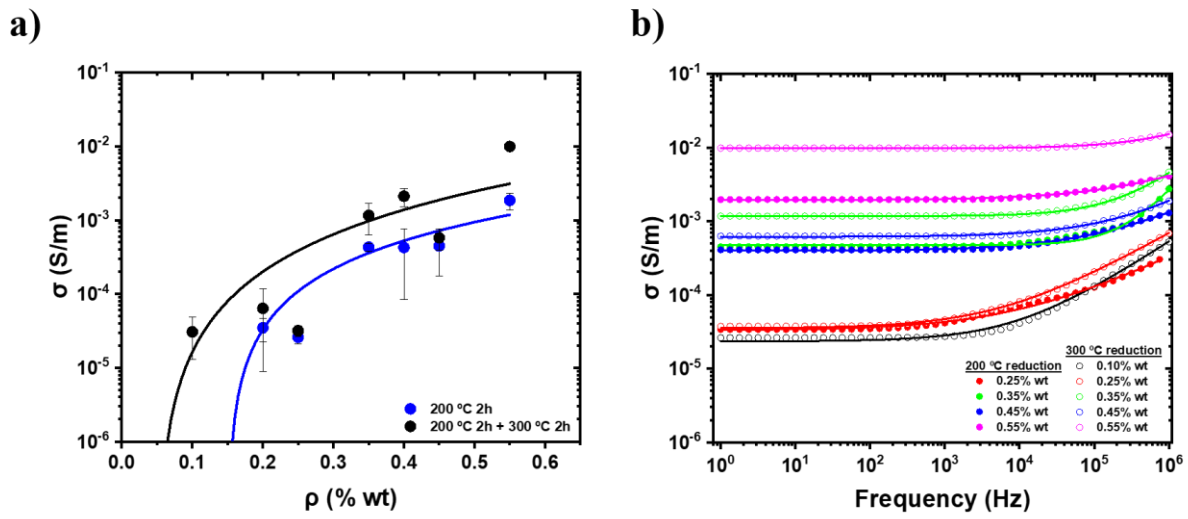

Figure 9. **a)** Electrical conductivity as a function of the weight fraction of GO for the nanocomposites reduced at 200°C for 2h and at 200°C for 2h plus 300 ºC for 2h. The data are fitted by the scaling Equation (1). **b)** Frequency dependence of the alternating current conductivity of the nanocomposites before and after the thermal treatments.

We observe that the nanocomposite becomes conductive with the reduction of GO. Factors deduced from the fitting with Equation (2) are given in Table 1. The conductivity shows a typical percolation behavior. The critical exponent *t* of the two fits is close to 2, as expected for percolation systems in three dimensions[32].

The GO was first reduced at 200°C for two hours. The percolation threshold deduced from the fits of the conductivity data is found to be 0.15% wt. This is lower than previous studies on conductive GO and rGO-based composites[18,24] and actually comparable to the percolation threshold of composites loaded with MWCNTs[12-14,17]. The maximum conductivity achieved at 0.55% wt of GO is $9.93 \cdot 10^{-3}$ S m^{-1}. This value is higher than those found by Qian et al.[18] and Chiappone et al.[24] However, it is slightly smaller than the values obtained for MWCNT-based composites. From a more general point of view, the percolation threshold of overlapping ellipsoids is expected to scale with the aspect ratio of the particles with a prefactor actually close to 1[33] . This scaling is in agreement with the so-called excluded volume model. Here, considering the graphene sheets as oblate ellipsoids with large aspect ratio one could expect that $\rho_c \sim \frac{l}{D}$, where *l* and *D* are the thickness and diameter of the graphene sheets. Taking reasonable values for *D*=1μm and *l*=0.4nm, the excluded volume would predict a percolation threshold of about 0.04% vol, which would correspond to a weight fraction of nearly 0.02% wt assuming a density of 2g cm^{-3} for GO materials. This expected value is somewhat lower than

that experimentally observed. Nevertheless, actual graphene sheets do not overlap in reality. It has been shown that the excluded volume model is not applicable to 2D non-penetrable particles, while it remains suitable for 1D objects[25,34]. In the case of 2D particles, correlation of orientations lead to an increase of the actual percolation threshold.

Table 1. The electrical properties of the rGO-based composites depend on the thermal annealing temperature. Fits to equation (1).

Thermal annealing (ºC)	σ_{max} **(S m^{-1})**	σ_0 **(S m^{-1})**	ρ_c **(% wt)**	t
200	$9.93 \cdot 10^{-3}$	$5.71 \cdot 10^{-3}$	0.15	1.72
300	$1.2 \cdot 10^{-2}$	$6.85 \cdot 10^{-3}$	0.05	1.93

After a second thermal annealing at 300 ºC for two hours. We see a decrease in the percolation threshold (0.05% wt), and an increase in the electrical conductivity (Figure 9). This behavior is likely due to two factors: a further reduction of the GO sheets due to the increase in temperature, and to an improvement of the rGO inter-layer electrical contacts. Indeed, the matrix can potentially relax at high temperatures so that rGO can approach each other more closely in response to van der Waals interactions. Even minute changes in the interparticle spacing can result in significant decreases in the contact resistances between neighboring particles, electron-tunneling being the main mechanism of conduction in the present composites. Changes in the tunneling distance and electrical connectivity criteria can result in variations of the percolation threshold[35,36].

3. Conclusion

We have developed a new strategy for making 3D conductive composites by DLP. Monolayer GO-acrylic resin mixtures were formulated. Monolayer GO liquid crystal was used without any drying stage during all processes to achieve UV-transparent resins. The Jacobs working curves and viscoelastic properties of the formulations have been studied to validate their 3D printability. The weak UV absorption and scattering of GO make the present formulations much more suitable for DLP than other conductive formulations. Taking advantage of the high-temperature resistance of the acrylic resin, we are able to efficiently reduce *in-situ* GO into rGO. This efficient reduction allowed highly conductive materials to be

3D printed. The present method can be useful in future potential applications for which electrical conductivity is needed, from antistatic materials[5–8] to sensors and soft robotics [37] through microwave absorption[38–40].

4. Experimental Section

Materials:

Aqueous GO solutions at 0.4% wt and 2.5% wt were purchased from Graphenea (Spain). According to the datasheet, the 2.5% wt solution contains GO flakes with a lateral size of 6–33 μm. The 0.4% wt solution contains GO flakes with a particle size of >10 μm. Bile salts were purchased from Fluka. Acrylic-based photocurable commercial resin Industrial Blend (IB) was purchased from FunToDo. Ethanol (EtOH) and isopropanol (IPA) purchased from Carlo Ebra Reagents were used as received.

Formulation:

Ethanol is added to the 2.5% wt GO solution to dilute the GO materials down to 0.4% wt. This solution is sonicated (Branson digital sonifier 450) in order to homogenize the suspension and disrupt possible aggregates with a sonication tip (tapped exponential horn 13 mm) for 30 minutes, amplitude set to 25% with pulses of 0.5 s on, and 0.2 s off. The resulting solution is centrifuged at 30,000 g for 30 minutes in an ultracentrifuge (Beckman coulter). From this, a concentrated slurry at 2.40% wt of GO monolayers (measured by dry extract) in an ethanol-rich solution (85% wt) is obtained. Ethanol, in contrast to pure water, is soluble in the IB resin. It can thus serve as an intermediate solvent to disperse GO monolayers in the resin without any drying step. For this, the slurry is directly mixed with the resin using a light-opaque container. The mixture is homogenized by sonication with a tip (microtip 3.2 mm) for 30 minutes, an amplitude set at 30%, and pulses of 0.5s on and 0.2s off.

GO solutions for UV-vis characterizations are prepared as follows. A 0.4%wt GO aqueous solution is diluted down to 0.005% wt by adding distilled water. The added water contains 0.35% wt of bile salt surfactants. These compounds are expected to stabilize the GO flakes in water as they become hydrophobic upon reduction. Thermal reduction of GO, to yield rGO, is done by pouring 20 mL of the solution into an autoclave and heating it for 1h at 90 ºC. The color of the sample turns dark black during the reduction reaction. Bile salt surfactants are found to be particularly efficient at stabilizing rGO in water [41]. The solution is indeed found to remain stable without any aggregation or sedimentation of the rGO particles.

The rGO powder was prepared by thermal reduction of GO. As before, we heat up to 90 ºC for 1h the 0.4% wt GO aqueous solution in the autoclave. After that, we evaporate the water by heating it at the same temperature without the cover. Then, the powder was recuperated and added to the resin. The mixture is homogenized by sonication with a tip (microtip 3.2 mm) for 30 minutes, an amplitude set at 30%, and pulses of 0.5s on and 0.2s off.

The MWCNTs powder is directly added to resin and dispersed by tip sonication. For that, a Branson digital sonifier 450 is used in order to homogenize the suspension and disrupt the CNT aggregates with a sonication tip tapped exponential horn 13 mm for 1 hour, amplitude set to 45% with pulses of 0.5 s on, and 0.2 s off. Finally, to remove the bubbles formed during the sonication, the formulation is put under vacuum for 2 hours.

3D printing:

The IB/GO formulation is poured into the tank of the DLP 3D printer Phrozen Sonic Mini 4k. This printer operates with UV irradiation at a wavelength of 405 nm.

A printing layer thickness of 25 µm is selected along with an irradiation time of 10s. As explained further, these values have been chosen after characterizations of the so-called Jacob's curves. Once printed, the IB/GO composite is soaked in an IPA bath for 15 minutes to remove the non-reticulated resin. It is then placed in a UV irradiation chamber (UltraV360) for 30 minutes to complete cross-linking of the resin. After that, the obtained IB/GO 3D printed samples were thermally reduced in air at 200°C for 2 h and subsequently, at 300 ºC for 2 h. The thermal treatment converted the 3D-printed IB/GO into an IB/rGO conductive nanocomposite.

Characterizations:

The quality of the GO dispersion in the commercial resin was assessed by optical microscopy (Leica DM 2500P). The thermal stability of the resin has been characterized by thermogravimetric analysis (TGA) (TA TGA 5500). About 5 mg of sample were loaded into the aluminum bread and heated from room temperature up to 800ºC under air.

The UV–Visible spectra (Jasco V-730) of GO and rGO were recorded to compare the absorbance at 405 nm. All the experiments were performed with samples in PMMA cuvettes.

The sudy of the Jacobs curves, the formulations have been poured into the printing tank and 2x2 mm square patterns have been irradiated for different times. The power of the LCD's 3D printer has been measured with a Thorlab PM1000A power meter. It is 1.27 mW cm^{-2}. After irradiation, the non-crosslinked formulation was rinsed and removed with 2-propanol. The thickness of the photopolymerized resin was measured with a caliper.

The rheological measurements were performed at 25ºC using a controlled strain rheometer (TA AR2000) with a 40mm and 2º cone-plate geometry. The rheological tests were performed in the linear viscoelastic regime determined from steady state flow experiments. The frequencies were in the range of 0.1 to 100 s^{-1}.

The tensile mechanical properties of the composite before and after the heat treatments have been measured with a tensile test Zwick Z2S instrument with a 1 kN force sensor. ASTM D638 Type IV samples have been stretched at a speed of 1 mm/min to obtain the stress □ (MPa) as a function of strain ε (%). Young's modulus *E* was calculated from the slope of the stress-strain curve at small strains. The electrical conductivity of the thermally treated composites has been measured by a two-point method using a MX24B multimeter and an impedance analyzer (7260 Impedance Analyzer, Materials Mates Italia) under a voltage of 5 V in a frequency range of 1 Hz – 10^6 Hz. Silver paint has been used in order to ensure good electrical contact between the sample and the electrodes.

Acknowledgments

Funding from the AID (Agence Innovation Défense) and the Nouvelle Aquitaine Region are acknowledged.

Received: ((will be filled in by the editorial staff))

Revised: ((will be filled in by the editorial staff))

Published online: ((will be filled in by the editorial staff))

References

[1] R. L. Truby, J. A. Lewis, *Nature* **2016**, *540*, 371.

[2] R. D. Farahani, M. Dubé, D. Therriault, *Adv. Mater.* **2016**, *28*, 5794.

[3] E. Fantino, A. Chiappone, I. Roppolo, D. Manfredi, R. Bongiovanni, C. F. Pirri, F. Calignano, *Adv. Mater.* **2016**, *28*, 3712.

[4] P. Blyweert, V. Nicolas, V. Fierro, A. Celzard, *Carbon* **2021**, *183*, 449.

[5] H. Abbasi, M. Antunes, J. I. Velasco, *Progress in Materials Science* **2019**, *103*, 319.

[6] N. Bagotia, V. Choudhary, D. K. Sharma, *Polym Adv Technol* **2018**, *29*, 1547.

[7] S. Ghoshal, *Fibers* **2017**, *5*, 40.

[8] A. Kausar, I. Rafique, B. Muhammad, *Polymer-Plastics Technology and Engineering* **2016**, *55*, 1167.

[9] A. Celzard, E. McRae, C. Deleuze, M. Dufort, G. Furdin, J. F. Marêché, *Phys. Rev. B* **1996**, *53*, 6209.

[10] T. Schilling, M. A. Miller, P. van der Schoot, *EPL* **2015**, *111*, 56004.

[11] T. Schilling, S. Jungblut, M. A. Miller, *Phys. Rev. Lett.* **2007**, *98*, 108303.

[12] A. Cortés, X. F. Sánchez-Romate, A. Jiménez-Suárez, M. Campo, A. Ureña, S. G. Prolongo, *Polymers* **2020**, *12*, 975.

[13] A. Cortés, A. Cosola, M. Sangermano, M. Campo, S. González Prolongo, C. F. Pirri, A. Jiménez‐Suárez, A. Chiappone, *Adv. Funct. Mater.* **2021**, *31*, 2106774.

[14] G. Gonzalez, A. Chiappone, I. Roppolo, E. Fantino, V. Bertana, F. Perrucci, L. Scaltrito, F. Pirri, M. Sangermano, *Polymer* **2017**, *109*, 246.

[15] T. Xiao, C. Qian, R. Yin, K. Wang, Y. Gao, F. Xuan, *Adv. Mater. Technol.* **2021**, *6*, 2000745.

[16] A. S. De León, S. I. Molina, *Polymers* **2020**, *12*, 1103.

[17] Q. Mu, L. Wang, C. K. Dunn, X. Kuang, F. Duan, Z. Zhang, H. J. Qi, T. Wang, *Additive Manufacturing* **2017**, *18*, 74.

[18] C. Qian, T. Xiao, Y. Chen, N. Wang, B. Li, Y. Gao, *Adv Eng Mater* **2021**, 2101068.

[19] S. Pei, H.-M. Cheng, *Carbon* **2012**, *50*, 3210.

[20] D.-D. Zhang, S.-Z. Zu, B.-H. Han, **2009**, 8.

[21] L. Shen, D. Wang, Z. Jin, L. Che, N. Cai, Y. Wang, Y. Lu, *Funct. Mater. Lett.* **2019**, *12*, 1950043.

[22] T. Tene, M. Guevara, A. Valarezo, O. Salguero, F. Arias Arias, M. Arias, A. Scarcello, L. S. Caputi, C. Vacacela Gomez, *Nanomaterials* **2021**, *11*, 1035.

[23] H. Huang, H. Park, J. Huang, *Chem* **2022**, S2451929422002704.

[24] A. Chiappone, I. Roppolo, E. Naretto, E. Fantino, F. Calignano, M. Sangermano, F. Pirri, *Composites Part B: Engineering* **2017**, *124*, 9.

[25] J. Yuan, A. Luna, W. Neri, C. Zakri, T. Schilling, A. Colin, P. Poulin, *Nat Commun* **2015**, *6*, 8700.

[26] M. J Griffith; J. Halloran, *J. Am. Ceram. Soc.* **1996**, 79, 2601**.**

[27] C. Hinczewski, S. Corbel; T. Chartier, *J. Eur. Ceram. Soc.* **1998**, 18, 583**..**

[28] S. Zakeri, M. Vippola, E. Levänen, *Additive Manufacturing* **2020**, *35*, 101177.

[29] K. Kirkwood, D. Stewart; C. Imrie, *J. polym. Sci. part A: Polym. Chem.* **1997**, 35, 3323.

[30] P. J. Krusic, E. Wasserman, P. N. Keizer, J. . R. Morton, K. P. Preston, *Science* **1991**, *254*, 1183.

[31] J. Madrid‐Wolff, A. Boniface, D. Loterie, P. Delrot, C. Moser, *Advanced Science* **2022**, *9*, 2105144.

[32] M. Badard, A. Combessis, A. Allais, L. Flandin, *Materials Chemistry and Physics* **2017**, *191*, 89.

[33] E. J. Garboczi, K. A. Snyder, J. F. Douglas, M. F. Thorpe, *Physical Review E* **1995**, 52 (1), 819-828.

[34] M. Mathew, T. Schilling, M. Oettel, *Physical Review E* **2012**, 85 (6).

[35] Y. Zare, K. Y. Rhee, *RSC Adv.* **2017**, *7*, 34912.

[36] N. Johner, C. Grimaldi, I. Balberg, P. Ryser, *Phys. Rev. B* **2008**, *77*, 174204.

[37] G.-X. Zhou, Y.-G. Yu, Z.-H. Yang, D.-C. Jia, P. Poulin, Y. Zhou, J. Zhong, *ACS Nano* **2022**, 10.

[38] F. Qin, C. Brosseau, *Journal of Applied Physics* **2012**, *111*, 061301.

[39] X. Bai, Y. Zhai, Y. Zhang, *J. Phys. Chem. C* **2011**, *115*, 11673.

[40] C. Wang, X. Han, P. Xu, X. Zhang, Y. Du, S. Hu, J. Wang, X. Wang, *Appl. Phys. Lett.* **2011**, *98*, 072906.

[41] C. Zamora-Ledezma, N. Puech, G. G. Wallace, S. Gambhir, C. Blanc, E. Anglaret, P. Poulin, *J. Phys. Chem. Lett.* **2012**, 6.

[42] J. Bennett, *Additive Manufacturing* **2017**, *18*, 203.